Badas, M.G., Ferrari, S., Garau, M., Querzoli, G.

On the effect of gable roof on natural ventilation in two-dimensional urban canyons (2017)

Journal of Wind Engineering and Industrial Aerodynamics, 162, pp. 24-34. DOI: 10.1016/j.jweia.2017.01.006

PRE-PRINT

On the effect of gable roof on natural ventilation in two-dimensional urban canyons

Maria Grazia Badas[a], Simone Ferrari[a], Michela Garau[a], Giorgio Querzoli[a]

[a] DICAAR, Università degli studi di Cagliari, Via Marengo 2, 09128, Cagliari, Italy

Corresponding author: Giorgio Querzoli - querzoli@unica.it

Abstract

Flow regimes occurring in urban canyons are strongly influenced by the geometrical shape of the buildings; however, fluid dynamic investigations are typically carried out using parallelepiped obstacles. The present study is focused on assessing the effect of gable roofs on the flow regimes characterizing urban canyons (skimming flow, wake interference, isolated roughness) and the implications in terms of integral parameters (air exchange rate and friction factor), which are useful in practical applications. Numerical simulations are performed by means of RANS modeling of idealized two dimensional urban canyons between series of identical gable roof buildings with pitch ranging from 0° up to 40°, and wind direction perpendicular to the canyon axis. Simulations performed for different canyon aspect ratios show the key role played by the roof pitch in enhancing turbulence and in increasing ventilation, in particular for narrow canyons. Furthermore, turbulence-driven ventilation is observed to be related to the square root of the friction coefficient by a single linear relation, despite of the roof pitch. These results may have an impact on design and planning strategies aimed at enhancing natural ventilation and promoting efficient pollutant and heat dispersion in urban areas.

1. Introduction

The fluid dynamic interaction between street canyons and the wind in the overlaying boundary layer plays a fundamental role in the determination of the living standard in the urban environment since it contributes to mitigate the degradation of air quality at the street level caused by vehicular emissions by promoting the removal of polluted air from the canyon and its substitution with fresh air. Therefore, the assessment of air ventilation in street canyons is an important tool in urban planning and air quality control in high-density cities (Fernando et al., 2001; Ng, 2009; Yazid et al., 2014).

Most of laboratory (Ahmad et al., 2005; Di Bernardino et al., 2015a, 2015b; Neophytou et al., 2014) and numerical (Ho et al., 2015; Hunter et al., 1992, 1990) studies on the fluid dynamics of the Urban Canyons (UCs) focused on the dependence on the spacing and height of buildings. They

represented the buildings by its simplest geometrical schematization, parallelepiped obstacles, without going in further geometrical details, thus reproducing only the case of flat roof buildings. Also some field experiments focused on the same build shape (Zajic et al., 2010). However, other roof shapes are widespread in cities. Particularly in the regions of high rain or snowfall, most of the buildings have pitched roofs and, in some areas, building codes prescribe a minimum slope.

The shape of the obstacles, and in particular the presence of a pitched roof, causes deep modifications in the urban roughness sublayer. Specifically, Rafaidilis (1997) compared, by means of laboratory experiments, two dimensional street canyons between buildings with flat and gable roof (45° slope) considering two different canyon aspect ratios and proposing the idea that roof shape plays a predominant role in controlling natural wind ventilation in the upper part of the urban canyons.Afterwards, several experimental (Kastner-Klein and Plate, 1999) and numerical simulations (Huang et al., 2009; Takano and Moonen, 2013; Xie et al., 2005; Yassin, 2011), mainly focused on air quality, indicated that the shape of adjacent buildings could be an effective element to reduce pollution within street canyons. Recently, Ozmen et al. (2016) investigated the effect of differently pitched gable roof on an isolated building. Actually, despite these works suggest the importance of the roof shape, there is no systematic study of Rafaidilis intuition in the basic case of a regular array of gable roof buildings forming a series of urban canyons.

The present paper aims at filling this gap with a parametric analysis of the dependence of the flow field in the urban roughness sublayer, and canyon ventilation, on the roof slope and aspect ratio: in particular, the roof slope was gradually varied between 0° and 40°, in order to both cover a wide range of real building's roof pitches and unveil its influence on the ventilation in the urban canyon. Actually, literature works (Oke, 1988; Hunter et al, 1990; Zajic 2010) showed that, in addition to canyon aspect ratio, also the length of the buildings, L, plays an important role in tuning the transition between the different flow regimes. However, in order to focus on a limited number of parameters, we chose to analyze the ideal case of the infinite-length urban canyon. As global descriptors of the fluid dynamics of the urban canyon, we refer to air exchange rate, representing the rate of air removal from a street canyon measured at the roof ridge level (Liu et al., 2005), and friction factor, which was considered to be a good predictor of the turbulent air exchange rate (Liu et al., 2015). In the following, after the description of the simulation methods (Section 2), we firstly compare the results (Section 3) with literature experimental data for model validation. Secondly, we present and analyze flow maps occurring in the different regimes characteristic of the UC and successively investigate how their occurrence affects global indexes, such as pressure coefficients, friction factor and air exchange coefficient. Discussion is carried out in Section 4, to then draw the conclusions (Section 5).

2. Methods

We simulated fully-developed steady turbulent flow over idealized two-dimensional canyons between an array of dual-pitched roof buildings, all with the same eave height, H, and square cross-section (building width $D = H$), while the width of the canyon, W, was varied between 0.4 and 12 H (hence the aspect ratio of the canyons, H/W, ranged from 0.08 up to 2.5). A uniform, indefinite succession of buildings was simulated by imposing periodic boundary conditions (BC) in the streamwise direction.

For each canyon width, the roof slope α was varied between 0° and 40° at 10° steps, covering a wide range of pitches adopted in real buildings. Analyzed configurations, although idealized, correspond to geometrical parameters ranging from isolated buildings to dense cities, hence spanning over the three characteristic flow regimes (isolated roughness, wake interference, skimming flow) described by Oke (1988) in case of flat roof buildings.

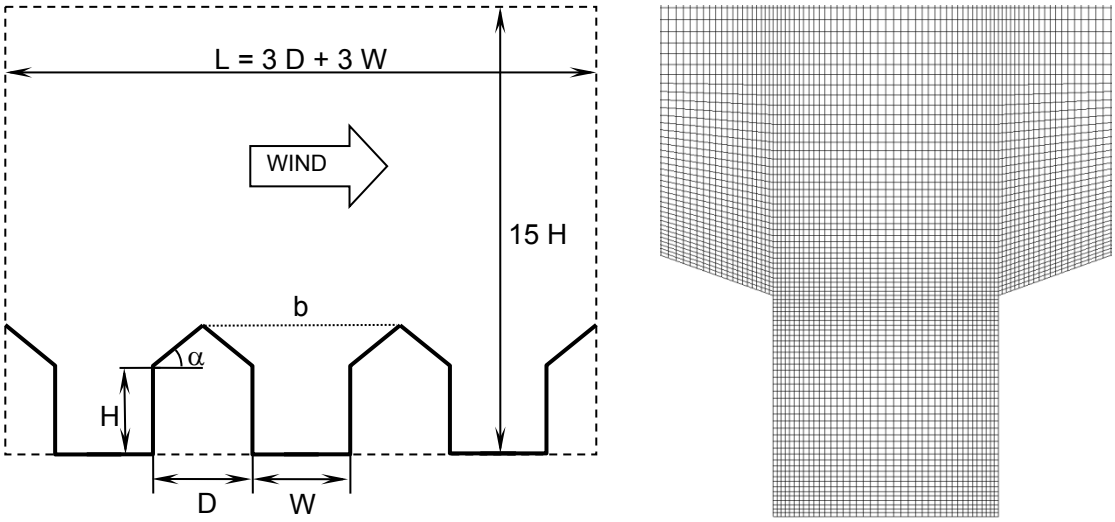

Figure 1. Sketch of the computational domain: H is the eave height, D the width of the building, α the roof slope, W the canyon width, $L = 3$ ($D + W$) the streamwise dimension of the domain, and b the line connecting the ridges (left panel). Inset of the mesh used for H/W=1 and α =20° (right panel).

For all the range of pitches considered, the simulation domain (sketched in Figure 1) is three canyons ($L = 3W + 3D$) long in the streamwise direction, and 15 H high (which fairly corresponds to 6 times the overall building height for the highest roof pitch, 40°). This fulfils the condition reported for flow simulation around buildings in the best practice guidelines (Franke et al., 2011; Tominaga et al., 2008), which require a vertical domain exceeding 6 overall building heights, in order to avoid unrealistic flow acceleration.

Wind direction is perpendicular to the canyon axis. For all the examined configurations the same Reynolds number, based on the building height and vertically averaged velocity, V, is imposed ($\mathrm{Re} = HV/\nu = 43000$). The pressure gradient between inlet and outlet is adjusted in order to assure the required flow rate. Snyder (1981) assumes a Reynolds number (based on the velocity of the unperturbed profile at the building height) greater than 15000 for the flow to be independent on Reynolds number. Here, due to the periodic BC, we do not have an unperturbed velocity profile,

however the chosen Re grants the fulfillment of the requirement and hence the independence.

Simulations were performed using the open source CFD library OpenFOAM 2.3 (Weller et al., 1998). Reynolds Averaged Navier-Stokes model (RANS) with two equation k-ε closure (Launder and Spalding, 1974) was set up. Since we are investigating the ideal case of infinite length buildings, the problem is two-dimensional, thus a 2-D formulation of RANS equations is used. We used simpleFoam, a steady state solver for incompressible turbulent flow, which applies the SIMPLE algorithm (Patankar and Spalding, 1972), and second order schemes for discretization. A threshold of 10^{-6} for scaled residuals was adopted as a convergence criterion (Franke et al., 2011).

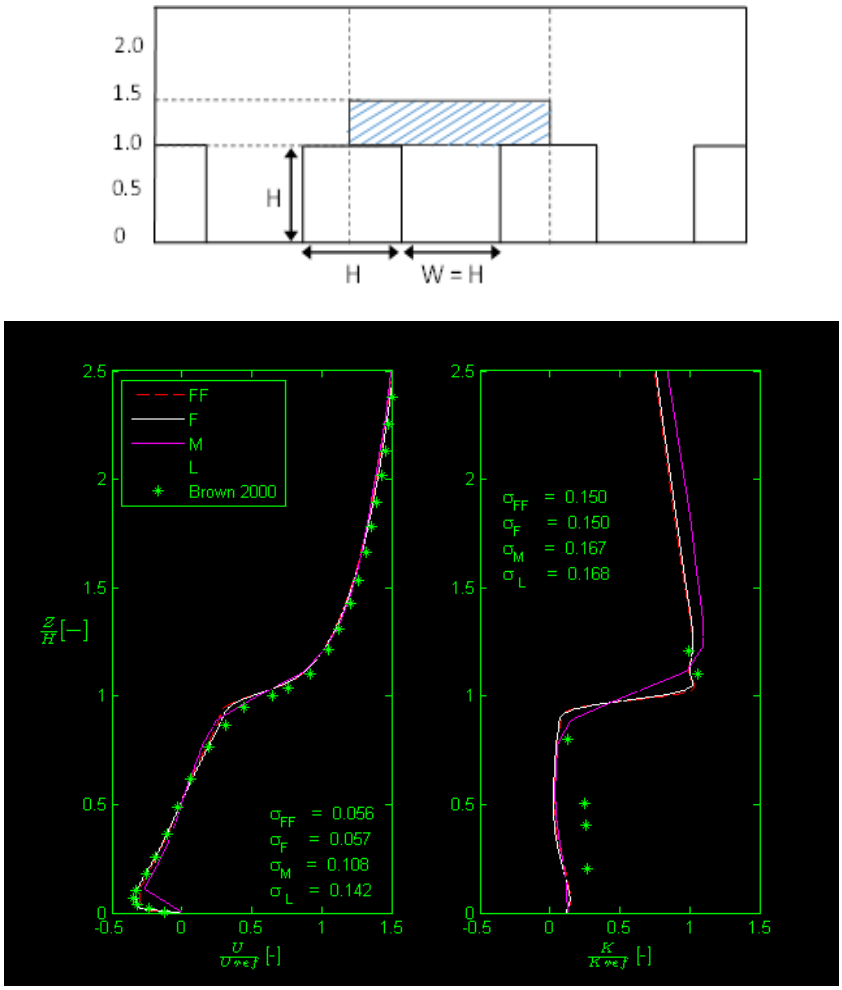

Figure 2. Comparison between present simulations performed with large (L), medium (M), fine (F) and very fine (FF) mesh and experiments (Brown et al., 2000) for the flat roof case and $H/W = 1$. Vertical profiles at the mid-canyon section ($x/H = 0$) of the streamwise mean velocity component (bottom-left panel) and turbulent kinetic energy, k, (bottom-right panel). Data are non-dimensionalized by means of the corresponding quantity averaged over the area shaded in the top panel (U_{ref} and k_{ref}, respectively). Root mean square (RMS) difference between the simulations with the four tested meshes and experimental data, σ, is displayed inside each plot.

As above mentioned, a periodic regular building arrangement was simulated. Therefore cyclic boundary conditions were imposed at the inlet and outlet for all the variables except for pressure, whose gradient is adjusted to obtain the required mean velocity at the inlet. The upper boundary of the computational domain was considered a symmetry plane. At ground and building surfaces no

slip condition was set. Neumann zero gradient conditions was imposed for pressure, whilst for turbulent quantities (kinetic energy, energy dissipation rate and turbulent viscosity) wall functions were applied.

In agreement with the above mentioned best practice guidelines, the mesh consists of hexahedral cells in order to introduce smaller truncation errors (Figure 1, right panel). The grid is stretched in x and z direction, keeping the stretching ratio between neighboring cells below 1.3. The inner region of the street canyons is discretized with 40 cells whose size is doubled, both in x and z directions, compared to the cells adjacent to the walls. For the analyzed cases, the number of cells ranges from 12,300 (for $H/W = 2.5$) up to 106,000 (for $H/W = 0.08$).

3. Results

3.1. Model validation

OpenFOAM has been extensively and successfully used to perform RANS simulations of the wind in urban environment (Franke et al., 2012; Hertwig et al., 2012); moreover, a similar OpenFOAM configuration was already proven to properly reproduce a two-dimensional periodic array of flat roof buildings (Takano and Moonen, 2013).

Model validation was here performed on the basis of experimental results reported in literature for UCs formed by 2D arrays of flat roof buildings in case of $H/W = 1$ and $H/D = 1$ both in wind tunnel (Brown et al., 2000) and water channel (Neophytou et al., 2014).

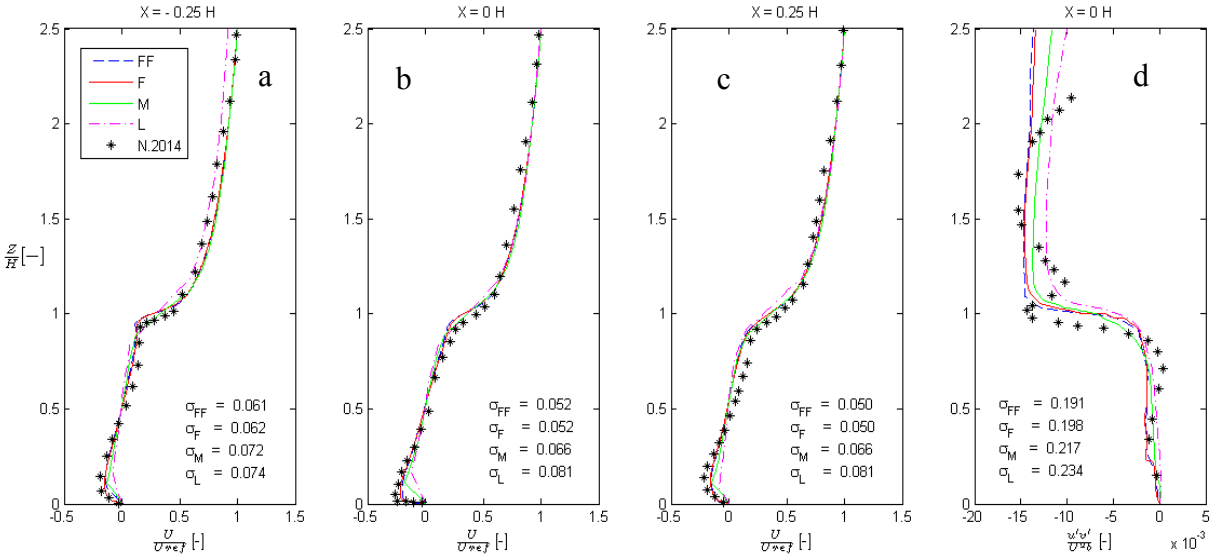

Figure 3. Three streamwise velocity component and $\overline{u'w'}$ compared with water channel experiments (Neophytou et al., 2014). Panels a-c report the vertical velocity profile at $x/H = -0.5$, $x/H = 0$ and $x/H = 0.5$, respectively. Velocity is made non-dimensional by the velocity U_{ref} averaged on the area depicted in the inset of Figure 2. Panel d reports $\overline{u'w'}$ made non-dimensional by the velocity, U_b, averaged above the buildings. Colored lines represent data obtained with large (L), medium (M), fine (F) and very fine (FF) mesh; black crosses: experimental data. RMS distance between the simulations with the four tested meshes and experimental data, σ, is displayed inside the plot.

Boundary conditions, numerical set up and convergence criterion are the same as described in

Section 2. Coherently with guidelines recommendations, four successive refined domain grids were tested, all with hexahedral cells, stretching ratios within 1.3, and cells in the core of the street canyons doubled with respect to the near wall ones. The coarsest mesh has 10 cells per building side, which is the suggested initial choice (Franke et al, 2011). Grids are obtained by doubling the cell number in each coordinate direction. Cell number for large (L), medium (M), fine (F) and very fine (FF) meshes is 860, 3440, 13760 and 55040 respectively.

Figure 2 displays the vertical profiles of streamwise mean velocity, U, and turbulent kinetic energy, k, at the mid-canyon section compared to wind tunnel data (Brown et al., 2000). All quantities are non-dimensionalized by means of the corresponding averages (U_{ref} and k_{ref}) computed over the region delimited by the coordinate ranges: $1.0\,H \leq z \leq 1.5\,H$ and $-1.0\,H \leq x \leq 1.0\,H$ (i.e. the shaded area in the top panel of Figure 2). Results obtained with the four tested meshes are reported.

In Figure 3, mean horizontal velocity and Reynolds shear stresses along vertical profiles within the canyon obtained with the four meshes are compared to water channel measurements (Neophytou et al., 2014). Reynolds shear stresses were estimated by means of the following equation:

$$\overline{u_i' u_j'} = -\nu_t \left(\frac{\partial \overline{u_i}}{\partial x_j} + \frac{\partial \overline{u_j}}{\partial x_i} \right) + \frac{2}{3}\delta_{ij} k \,,$$

where ν_t is the turbulent viscosity, computed as follows:

$$\nu_t = C_\mu \frac{k^2}{\varepsilon},$$

and C_μ=0.09 (Launder and Spalding, 1974).

Both in Figure 2 and 3, simulated data are mesh dependent up to fine grid, whilst profiles from fine (F) and very fine (FF) mesh collapse together and hence fine mesh was adopted in the present study. Streamwise velocity profile satisfyingly agrees with experimental data. The RMS differences between simulated and experimental data averaged on the profile, σ, is shown in each panel of Figures 2 and 3. Actually in the right panel of Figure 2, for a range of heights within the canyon, the turbulent kinetic energy appears to be underestimated by the model. In Figure 3, velocity profiles obtained with the fine grid collapse on the experimental data. Also Reynolds shear stresses are in satisfying agreement and RANS modeling reproduces the overall behavior of the experimental data.

3.2. Mean flow structure

In Figure 4-6, the mean velocity fields generated by flat and 30° slope roof buildings are compared for three different canyon aspect ratios (H/W = 1.00, H/W = 0.25 and H/W = 0.17) in terms of velocity magnitude, U, normalized by the free-stream velocity (computed at the top of the domain), U_f, and streamlines. UC aspect ratios have been chosen in order to span over the three characteristic regimes first demonstrated by Hussain and Lee (1980) and then described by Oke (1988).

For H/W = 1 (Figure 4), a stable single vortex is established in between the buildings, indicating the regime of skimming flow (SF), regardless the roof slope. In case of flat roof (left panel), the outer

stream is almost unperturbed, and characterized by straight, horizontal streamlines. The velocity magnitude increases steeply with the height and, at z = 3*H*, the free-stream value, U_f, is almost attained. Comparison with right panel shows that gable roof generate a perturbation that propagates significantly in the stream above the roof. In that case, streamlines are wavy also above the ridge of the roof, and a zone of reduced velocity zone extends upwards so that the velocity attained at the top of the plot (z = 3*H*) is much lower than in the flat roof case.

For *H*/*W* = 0.25 the Wake Interference (WI) flow regime is observed. Two main vortical structures are generated (Figure 5): the first due to separation at the leeward roof pitch and the second due to the flow separation on the windward wall. Comparison of left and right plot of Figure 5 shows that the slope of the roof tends to shift the centers of the vortices towards the middle of the UC. For this aspect ratio as well, the perturbation induced by the buildings propagates upwards, displaying wavy streamlines and a region of reduced velocity above the roof ridge, regardless the roof slope.

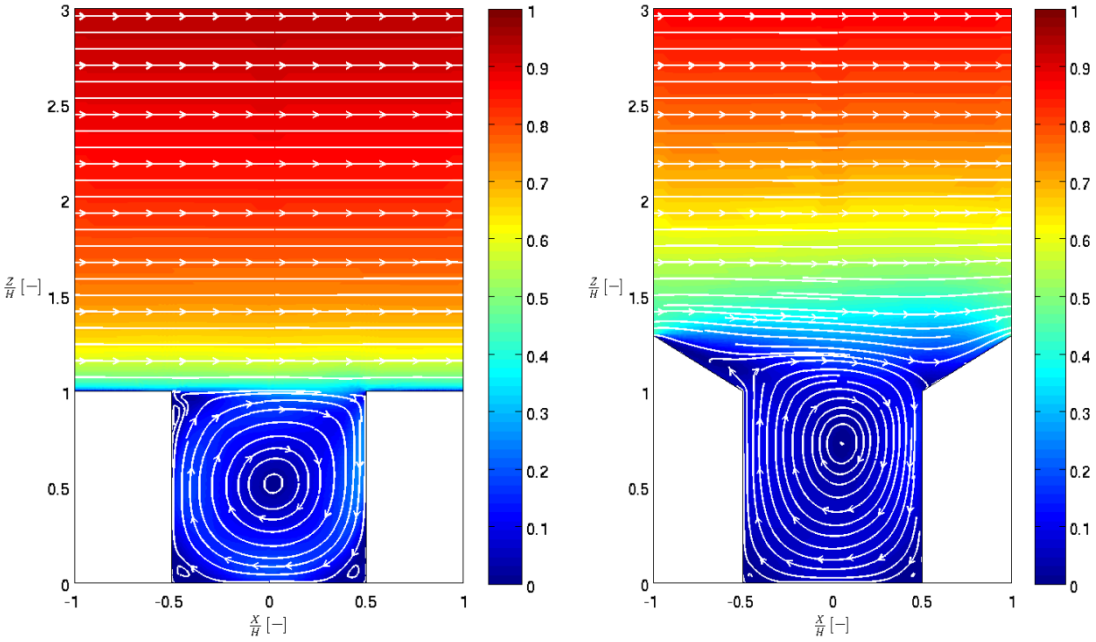

Figure 4. Mean velocity magnitude, *U*, made non-dimensional by the free-stream velocity, U_f, (color map) for *H*/*W* = 1.00. Flat roof case on the left and 30° roof slope on the right. Streamlines are drawn in white.

Also at *H*/*W* = 0.17 (Figure 6) the UC flow is characterized by two vortices separated by a region of non-recirculating flow (regime of Isolated Roughness flow, IR). As in the wake interference regime, the perturbation propagates above the roof height regardless the roof slope. However, the horizontal dimension of the recirculating vortices tends to be increased by the presence of a gable roof. As a consequence, the non-recirculating zone has a smaller extent with gable roof compared to flat roof buildings.

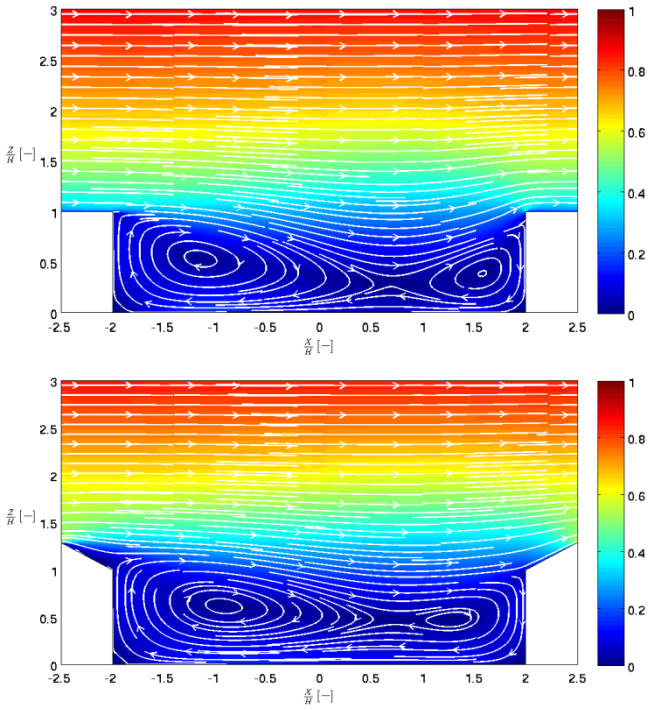

Figure 5. Mean velocity magnitude, U, made non-dimensional by the free-stream velocity, U_f, (color map) for $H/W = 0.25$. Flat roof case on the left and 30° roof slope on the right. Streamlines are drawn in white.

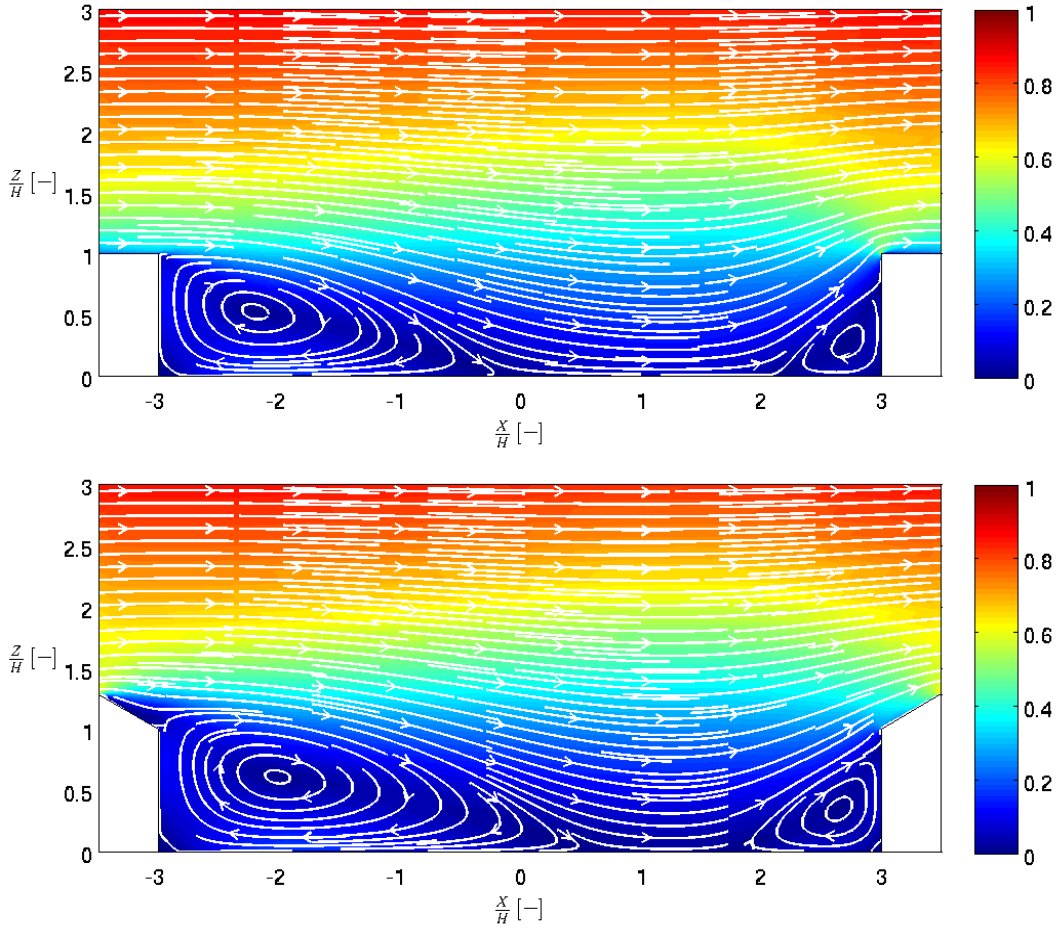

Figure 6. Mean velocity magnitude, U, made non-dimensional by the free-stream velocity, U_f, (color map) for $H/W = 0.17$. Flat roof case on the left and 30° roof slope on the right. Streamlines are drawn in white.

The maps of turbulent kinetic energy, k, normalized by the squared free-stream velocity, U_f^2, for the same conditions as above, are shown in Figures 7-9. In general, the turbulent kinetic energy is lower in the UC than in the above-roof stream. At $H/W = 1.00$, in regime of skimming flow (Figure 7), the turbulence levels are lower compared to the other regimes and there is a sharp separation between the values in the UC and above. However, the gable roof determines much higher values of k in the outer flow stream which propagates down to the eave height (z = H).

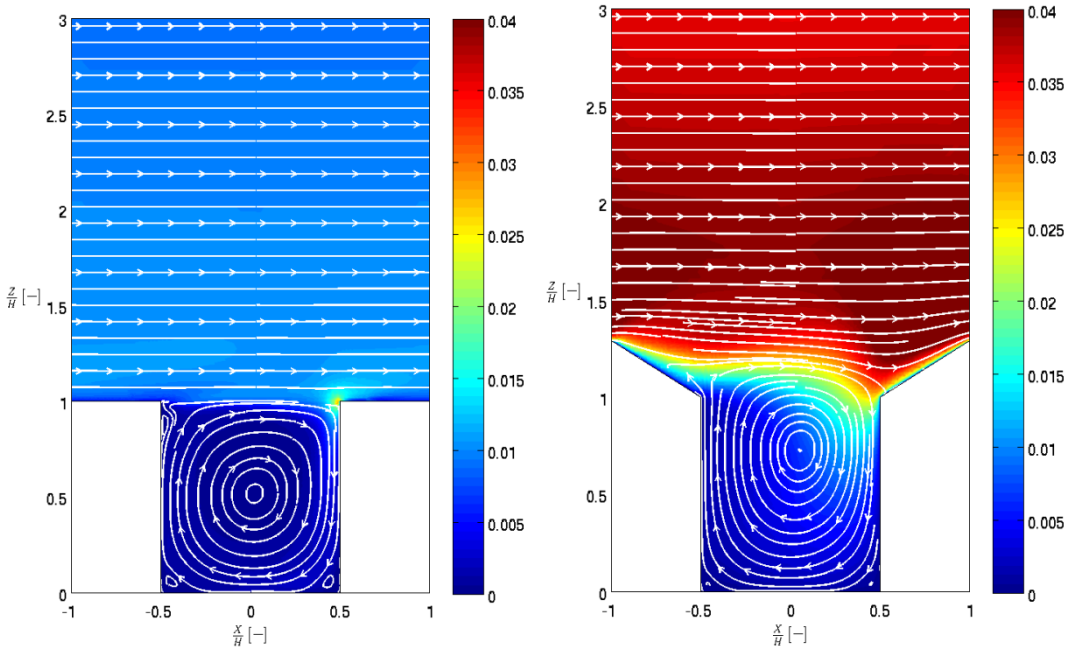

Figure 7. Turbulent kinetic energy, k, made non-dimensional by the squared free-stream velocity, U_f^2, (color map) for H/W = 1.00. Flat roof case on the left and 30° roof slope on the right. Streamlines are drawn in white.

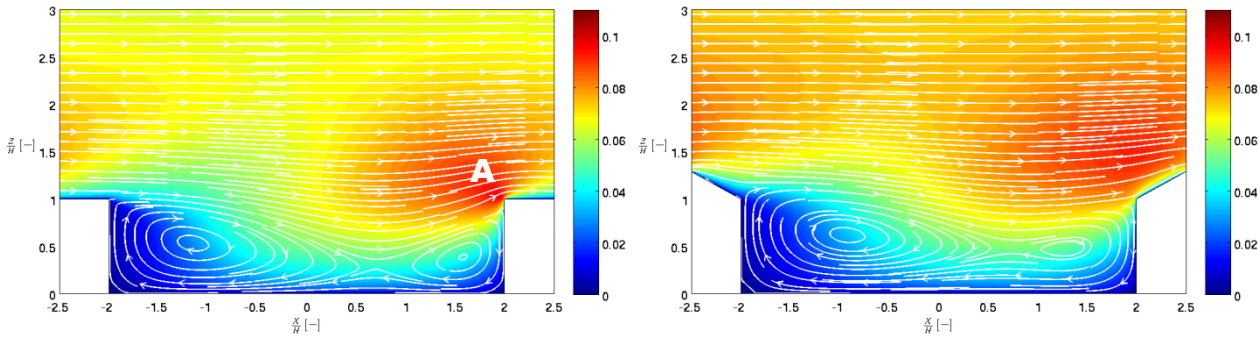

Figure 8. Turbulent kinetic, k, energy made non-dimensional by the squared free-stream velocity, U_f^2, (color map) for H/W = 0.25. Flat roof case on the left and 30° roof slope on the right. Streamlines are drawn in white.

In the wake interference regime (H/W = 0.25, Figure 8), the separation between the levels of turbulence above the roof height and below is smoother and a region of high turbulent kinetic energy values extends from the outer flow to the region of the UC between the two vortex cores. Compared to the flat roof, gable roof determines higher k values in the outer stream: the high level region which is apparent just above and upstream of the leeward eave in case of flat roof (indicated with **A** in the left panel of Figure 8) is much more extended and includes almost all the free stream

region in case of gable roof.

The scenario is quite similar also when the building separation is large enough to have isolated roughness regime (H/W = 0.17, Figure 9) with k values generally higher compared to H/W = 0.25 canyon. Also in this configuration, the gable roof promotes an increase of the turbulent kinetic energy and the broadening of the high-level region located just upstream and above the eave of the leeward building (indicated with **A** in the upper panel of Figure 9).

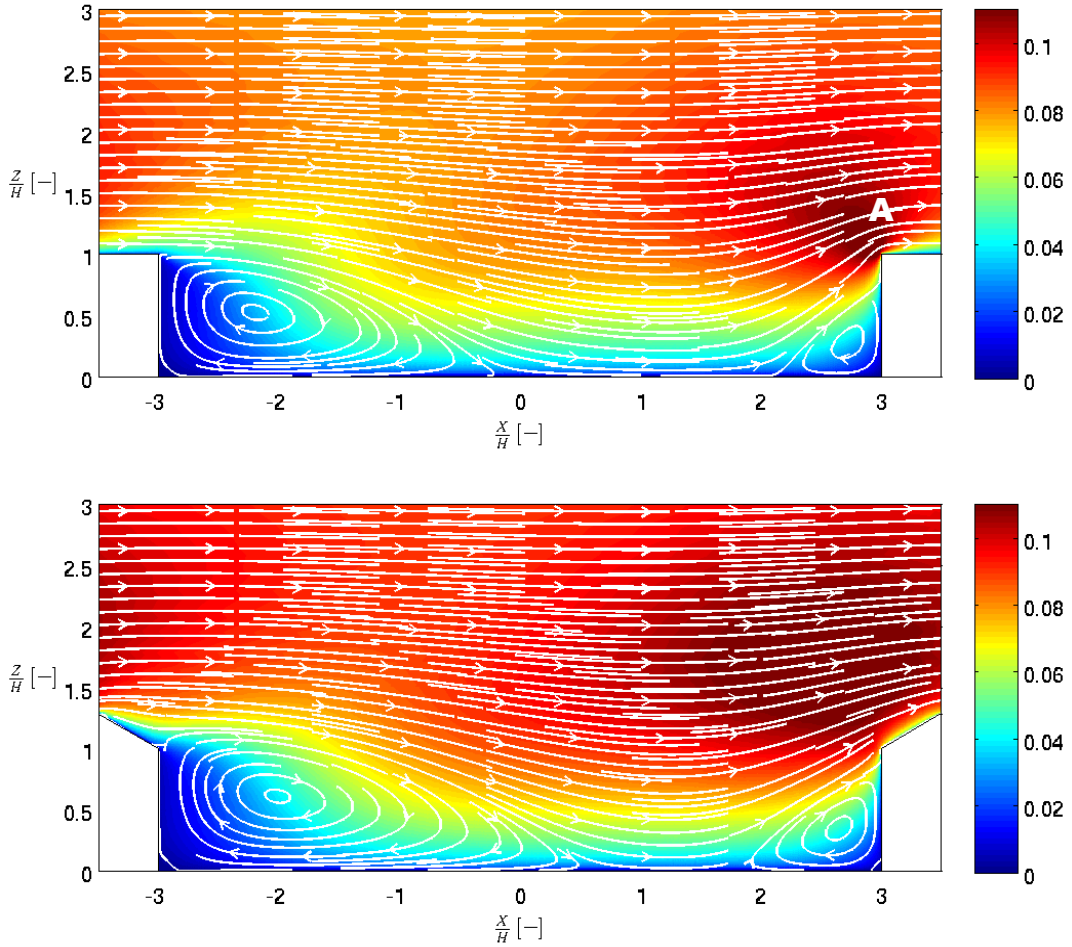

Figure 9. Turbulent kinetic energy, k, made non-dimensional by the squared free-stream velocity, U_f^2, (color map) for H/W = 0.17. Flat roof case on the left and 30° roof slope on the right. Streamlines are drawn in white.

3.3. Ventilation and friction coefficient

The analysis of the flow fields gives a clear picture of the phenomena; however, from a practical point of view, it is also important to understand how the integral parameters, often used to describe the salient characteristics of the flow, are affected by the shape of the roof of the buildings.

The air quality, the comfort at the street level and other important features of an UC depend essentially on the air exchanges between the canyon and the overlying boundary layer. In order to evaluate the performance of the analyzed cases from this point of view, we investigated the air-exchange rate, ACH (Ho et al., 2015), which is a measure of the rate of air removal from a street

canyon depending on the mean and turbulent flow ($\overline{ACH}$ and ACH', respectively). $\overline{ACH}$ is calculated by integrating the mean upward velocity, $\overline{w}_+$, at the roof ridge height:

$$\overline{ACH} = \int_b \overline{w}_+ dx$$

where b is the line connecting to consecutive ridges. Since we used a RANS simulation, we cannot estimate the instantaneous velocity fluctuations. Therefore, we evaluated the turbulent component ACH' as:

$$ACH' = \frac{1}{2}\int_b \sqrt{\overline{w'^2}}\, dx\,;$$

where the variance of the vertical velocity is estimated, under the assumption of isotropic turbulence, by Ho et al. (Ho et al., 2015):

$$\overline{w'^2} = -2\nu_t\left(\frac{\partial \overline{w}}{\partial z}\right) + \frac{2}{3}k\,.$$

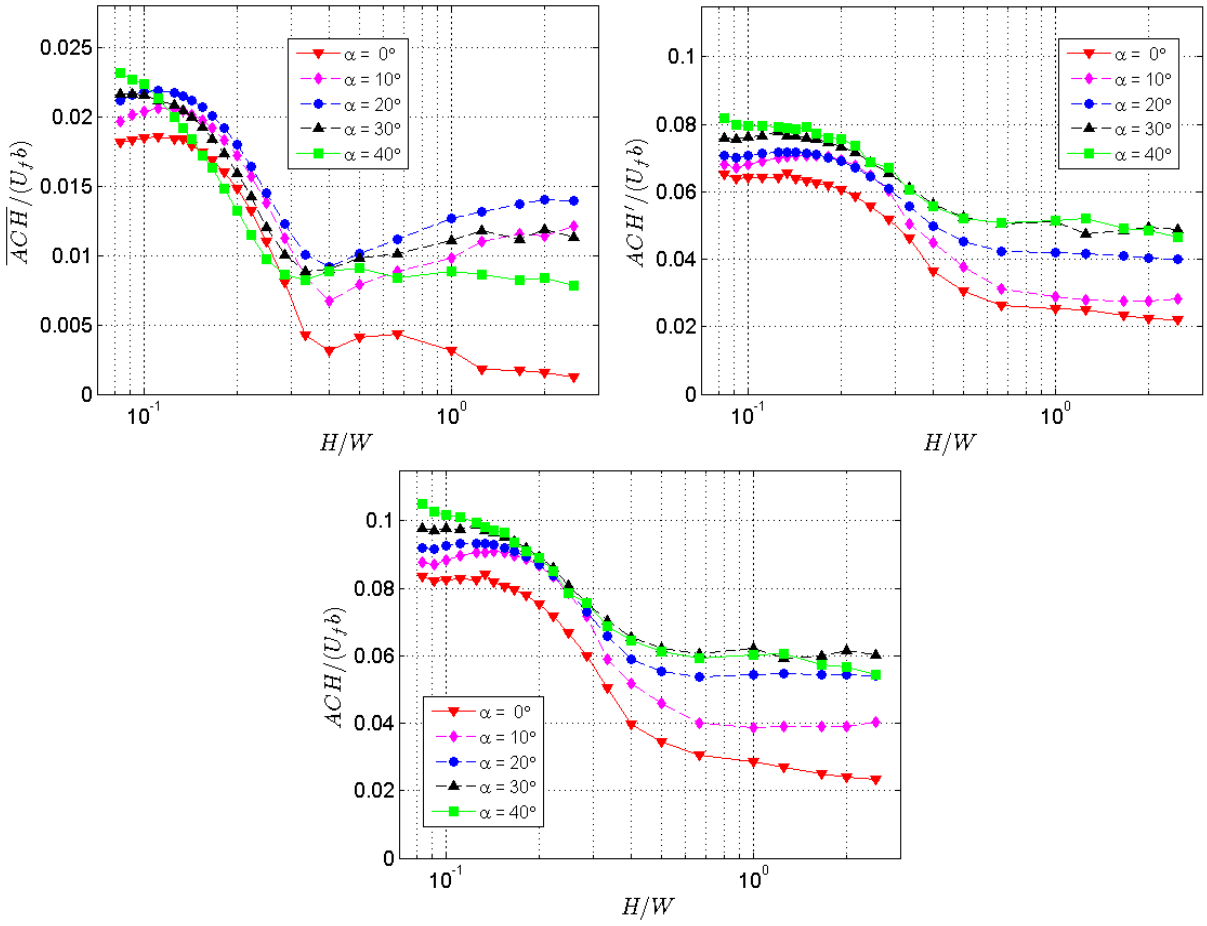

Figure 10. Non-dimensional ACH components versus the UC aspect ratio, H/W, for different roof slopes (mean component: top left panel; turbulent component: top right panel; total ACH: bottom panel).

Figure 10 shows ACH / (U_f b) and its components (mean and turbulent) as functions of the UC aspect ratio, H/W, for the different roof slopes. For all the examined simulations, ACH' typically exceeds the 70% of the total ACH, thus representing the dominant contribution.

All components of ACH, display some common features: a high-level region for low aspect ratios, a

region of low values at high aspect ratios and a descending trend in between. The air exchange rate, *ACH*, is increased by gable roofs regardless the slope and the aspect ratio. The difference is more significant in the range of the narrow canyons, mainly because of the lower contribution given by the mean flow in case of flat roof. The turbulent component tends to increase with the roof slope all over the *H*/*W* range, with saturation over 30°, so that the increase from 30° to 40° is nearly negligible. As a result, curves of total *ACH* for gable roofs collapse together in the intermediate, descending range of aspect ratios. Conversely, the pitch has a positive effect on *ACH* both in the high and low aspect-ratio ranges.

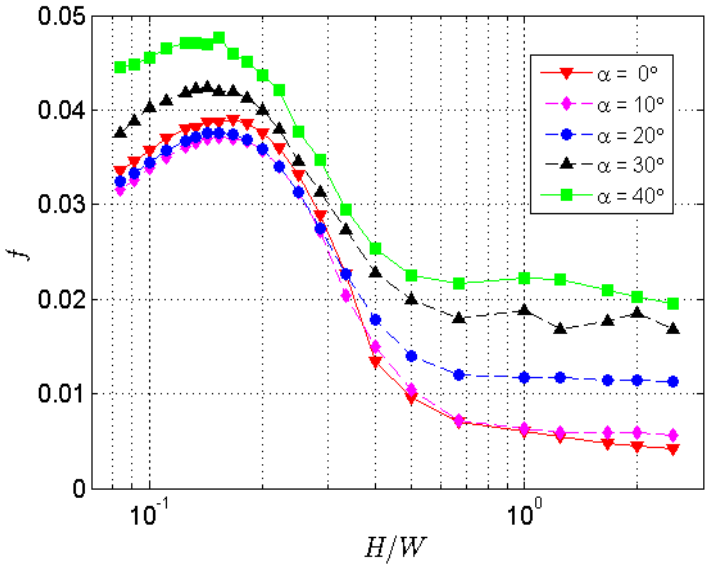

Figure 11. Friction coefficient, *f*, as a function of the UC aspect ratio, *H*/*W*, for different roof slopes.

We then analyzed the effect of roof slope on friction coefficient, *f*, which describes the aerodynamic resistance generated by the buildings, and is defined as:

$$f = \frac{\tau_w}{\frac{\rho V^2}{2}} = \frac{\frac{\Delta p}{L} H}{\frac{\rho V^2}{2}},$$

where τ_w is the mean wall shear stress, *V* the vertically averaged UBL velocity, $\Delta p / L$ is the mean pressure gradient in the streamwise direction across the computation domain, and ρ the fluid density.

Friction coefficient was analyzed for different pitches (Figure 11).

Also in this case all curves display a similar trend, regardless the roof slope: they attain a maximum, then descend quite steeply, and finally tend to an asymptotic value. Flat roof and 10° pitch curves are quite similar while, increasing further the roof slope, the curves are progressively shifted towards higher *f*.

Dimensional arguments suggest that the turbulent (and dominant) component of *ACH* is

proportional to the square root of the friction coefficient, $f^{1/2}$ (Liu et al., 2015). The relation can be useful for estimating the ventilation on the basis of the friction coefficient. We tested the above correlation in case of gable roof buildings by plotting $ACH' / (U_f b)$ against $f^{1/2}$ (Figure 12). All data are well aligned along a straight line intercepting the origin. A shape effect appears to be responsible for the slightly lower values observed for the flat roof case, due to the absence of the roof ridge. We computed the linear regression in the form $ACH' / (U_f b) = a f^{1/2}$ by means of the least squares method. The proportionality coefficient resulted $a = 0.3607$ (black line in Figure 12).

3.4. Wall pressure coefficient and flow regime transitions

The assessment of the transition among the three regimes is often based on the computation of the pressure coefficients, C_p, based on average pressures on the leeward and windward building walls delimiting the canyon (Hussain and Lee, 1980; Sini et al., 1996):

$$C_p = \frac{\frac{1}{H}\int_0^H p dz}{\frac{1}{2}\rho U_H^2}$$

where U_H indicates the mid-canyon velocity at z = H. Therefore it is interesting to analyze how the roof slope affects their behavior and, in turn, the transition between flow regimes.

Figure 13 shows pressure coefficients on the leeward (C_{pL}, left panel) and windward (C_{pW}, right panel) building walls versus H/W for the different roof slopes.

Windward pressure coefficients have a similar trend regardless the roof slope: for low aspect ratios (i.e. for wider canyons) C_{pW} is high, and then decreases down to another plateau at high H/W values, i.e. for narrow canyons. The same similarity in the overall trend is not observed in the leeward coefficients.

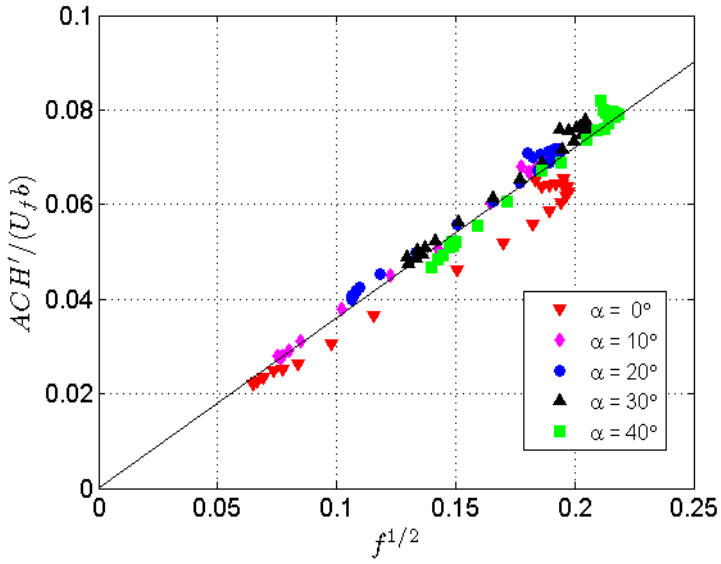

Figure 12. Non-dimensional turbulent air exchange rate as a function of friction coefficient, f, for all the investigated configurations. Black line represents the linear regression $ACH' / (U_f b) = 0.3607 f^{1/2}$.

Despite the general similarity, a clear relationship between roof angle and C_p does not seem to hold true at any range of H/W. C_{pL} exhibits different values not directly correlated to the roof slope. C_{pW} in wider canyons ($H/W \leq 0.15$) for low roof slope ($\alpha \leq 20°$) collapse together, whereas 30° and 40° configurations give higher values. In the intermediate range of H/W, all curves but the 30° roof slope case collapse. Finally, for narrower canyons (H/W $\geq$ 0.7), flat roof and 30° slope roof yield lower and highest values, respectively.

Transitions among the three characteristic fluid dynamic regimes are related to the slopes of these curves (Sini et al., 1996). In particular we focused on C_{pW}: the first slope change indicates the transition threshold from SF to WI, whereas the transition from the decreasing to the flat region identifies WI-to-IR transition.

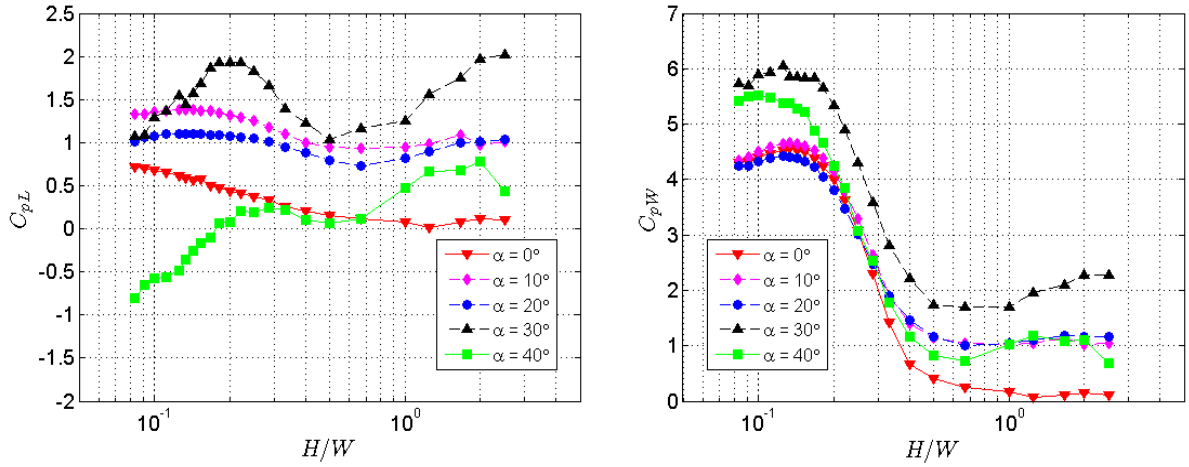

Figure 13. Left panel: pressure coefficients at the leeward wall, C_{pL} (left panel), and windward wall, C_{pW} (right panel), versus H/W for different roof slopes.

Changes of slope observed in Figure 13 are not significantly dependent on roof pitch, and typically gradual, so that thresholds cannot be identified without some uncertainty. The classification of the flow regimes following the above criteria furnishes a SF-to-WI transition at $H/W = 0.67$ and a WI-to-IR transition at $H/W = 0.12$, in agreement with Sini et al. (1996), irrespective of the roof slope.

The criterion based on the wall pressure coefficient is only indirect. Therefore, in order to get deeper insight in the phenomenon, we systematically inspected the streamlines of the velocity fields for all the aspect ratio - pitch combination and categorized the flows depending on their structure: the SF-to-WI transition was associated to the change from a single vortex (e.g. Figure 4) to a couple of vortices included in a single circulation region including the whole canyon (e.g. Figure 5), the transition from WI to IR was associated to the complete separation of the leeward and windward vortices with a corresponding reattachment and detachment of the flow from the ground (e.g. Figure 6). Results are reported in Figure 14: both the transitions are observed at slightly decreasing aspect ratios when pitch increases. The decrease of WI-to-IR transition can be explained by the increased vortex size observed for gable roof in figure 6. At the same time, the inclination of roof pitches seems to be favorable to the division of the single vortex typical of the SF regime, thus anticipating the transition. These H/W of transition from WI to IR regime educed from flow structure are not so

different from the prediction obtained using the wall pressure coefficient. Conversely, the criterion based on C_{pW} seems to overestimate significantly the aspect ratio of transition from SF to WI compared to the inspection of the velocity fields.

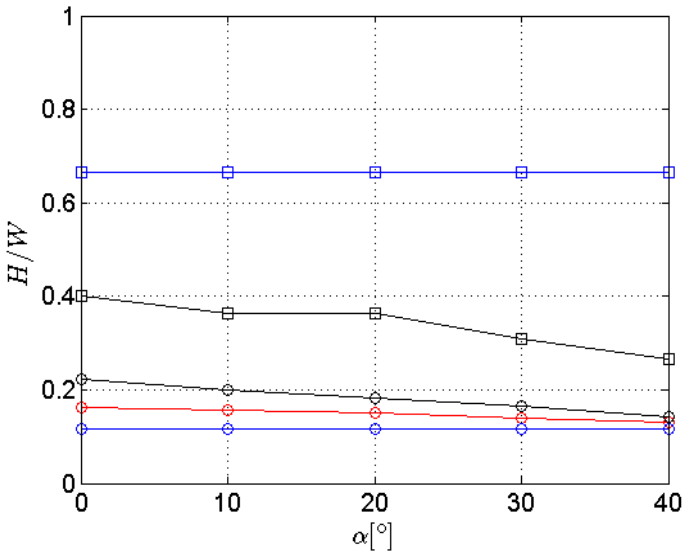

Figure 14. Aspect ratios, H/W, of regime transition for different roof slopes. Squares indicate transitions from Skimming-Flow to Wake-Interference regime; circles indicate the transition from Wake-Interference to Isolated-Roughness. Transitions identified by the structure of the velocity field are plotted in black; transitions identified by C_{pW} slope are plotted in blue. Red line indicates the aspect ratios corresponding to the maximum friction coefficient.

Actually, boundary layer modification due to regular wall roughness has also been investigated, both experimentally (Furuya et al., 1976) and numerically (Leonardi et al., 2004) in turbulent channel flows. Specifically, in this context isolated roughness and wake interference are referred to as k-type roughness, while skimming flow is indicated as d-type roughness (Jiménez, 2004; Perry et al., 1969). For regular arrays of square obstacles placed on the bottom of a channel, several authors (see Leonardi et al., 2007 and references therein) found a characteristic value of obstacle spacing, W/H close to 7 (corresponding to H/W = 0.14): at this distance skin frictional drag reaches its minimum while form drag achieves its maximum, and this condition corresponds to a modification in the coherent structures dominating the flow that maximizes the outward ejection of fluid from the cavity (Leonardi et al., 2004), whilst the transition from d-type to k-type roughness occurs when frictional drag becomes larger than pressure drag (Leonardi et al., 2007). Similar results were found for obstacles of different shapes, such as triangles or circles (Dritselis, 2014). However, to the best of authors' knowledge, the configuration here studied has been investigated previously neither in urban flow studies nor in other fluid mechanics contexts. Aspect ratios corresponding to the maximum friction coefficient (maxima of curves in Figure 11) are reported in Figure 14 by a red line: they identify the SF-to-WI threshold at intermediate values between the flow-structure and the C_{pW} based classifications, thus confirming that the classification based on f corresponds with the other two criteria.

4. Discussion

This study is aimed at investigating the influence of roof slope in modifying the flow regimes and the vertical air exchange rate (*ACH*) in a two-dimensional urban canyon between gable roof buildings, compared to flat roof configuration.

As postulated by Rafailidis (1997), roofs play a crucial role in modifying turbulence at the interface and hence have a deep impact on enhancing natural ventilation inside the canyon. Analysis of flow fields (Figures 4-9) shows that the presence of a gable roof has two main effects: firstly it enhances the turbulent kinetic energy, k, in the interfacial region between the eaves and the ridge height, regardless the aspect ratio, thus contributing to the ventilation of the UC (namely, increasing *ACH'*); secondly, it determines a significant perturbation of the mean velocity field and an increase of the air exchange rate due to the mean flow, $\overline{ACH}$, for narrows UCs (i.e at the high aspect ratios). As a result, a gable roof has a positive effect on the natural ventilation, and also small roof pitches produce a meaningful *ACH* increase. The ventilation is particularly enhanced for narrow canyons. From a practical point of view, this implies that a better *ACH* can be more efficiently achieved choosing a gable roof instead of widening the canyon.

The friction coefficient, f, is seen to increase with the roof pitch irrespective of the aspect ratio. The f curves appear to be more distant for larger aspect ratios (narrower canyons) when the obstacle shape is the key element for drag (form friction overcomes skin friction), whilst for smaller aspect ratios (larger building distances) the geometry plays a less important role and curves tend to collapse together (drag is mainly due to skin friction). Our results confirm, in the case of gable roof, the argument presented by Liu et al. (2015) predicting a linear relation between the square root of the friction coefficient, $f^{1/2}$, and the turbulent component of the air exchange rate. Therefore, the friction coefficient can be successfully used for the estimation of the turbulent ventilation of a UC.

Analysis of the velocity fields indicates that both transition thresholds are slightly decreasing with the roof slope. Comparison of different criteria of identification of the transition between the different fluid dynamic regimes points out a significant overestimation of SF-to-WI threshold by the pressure coefficient compared to the flow structure inspection. Conversely, all the proposed criteria yield WI-to-IR transition thresholds in reasonable agreement.

Limitation of the study are related to the simple configuration and to the modeling approach, as thoroughly discussed in the following. The study was performed on the ideal case of periodic conditions and infinitely long canyons. Generally, when L/H is greater than 7, canyons are referred to as long ones (Hunter et al, 1990), while for greater L/H values, modifications in the onset of the different regimes are less pronounced than in medium or short canyons. Hence, present simulation results are representative of transversal sections belonging to the central region of long canyons, where average velocity field and turbulence statistics can be assumed two-dimensional and corner effects are negligible. However, caution should be paid when applying these results to buildings of

finite length, yet being classified as long canyons.

Moreover, the wind is modeled here as perpendicular to the canyon axis, which corresponds to the worst condition for ventilation, since even a small deviation from normal direction changes dramatically the flow pattern determining a wind channeling which provides higher ventilation inside the canyon (Zajic et al, 2010).

The principal simplification in the adopted modeling approach is indeed linked to the choice of a RANS model, which depicts a statistically stationary picture and cannot capture the intermittent nature of the recirculation flow inside the canyon (Louka et al., 2000).

Nonetheless, as also stated in the recent paper by Blocken et al 2016, despite other simulation techniques (such as Large Eddy Simulation or laboratory simulations) are more accurate, the use of faster and less expensive techniques such as RANS modeling is valuable in the context of urban simulations.

Further, it should be noted that the standard k-ε parametrization we chose is not generally used in urban 3D modeling. However, it is often adopted in 2D configurations (Huang et al., 2009; Xie et al, 2005; Takano and Moonen 2013). We tested different closure parameterizations for the validation cases, which did not provide better performances with respect to standard k-ε closure. For example, tests performed with a RNG k-ε model (Yakhot and Orszag, 1986) on the experimental case reported in Figure 3 yield RMS differences of numerical from experimental data $\sigma = 0.062$, 0.052, 0.050, respectively for the vertical profiles of average stream-wise velocity at X/H = -0.25, 0.00, +0.25 (Figure 3 a, b and c). Furthermore, comparison of Reynolds shear stress profile at X/H = 0.00 (Figure 3d) furnishes $\sigma = 0.198$. These RMS differences are not significantly different from those obtained with the standard k-ε model and the chosen mesh, and reported in Figure 3. Therefore, discrepancies between present simulations and validation cases seem to be mainly ascribed to the empirical parameterization of the turbulent kinetic energy inherent in all RANS modeling.

Further LES analyses are currently being developed in order to better assess the role of three-dimensional turbulence structures and the intermittent recirculation behavior in enhancing air ventilation.

6. Conclusions

The shape of the buildings plays a key role in the fluid dynamics of urban canyons, which, in turn, is a key element in urban planning since it affects crucial factors such as air quality and pedestrian comfort. We investigated the urban canyon formed by gable roof buildings, which is a widespread typology in regions where snowing and intense raining are frequent. Although some authors pointed out the importance of the roof for the ventilation of the UC, to the extent of our knowledge, no systematic investigation were carried out so far.

Present results, in the ideal case of canyons of infinite length, indicate a moderate influence of roof slope in the aspect ratio thresholds separating fluid dynamic regimes. Nevertheless, the presence of a gable roof enhances meaningfully the air exchange between the canyon and the overlaying boundary layer, thus promoting pollutant and heat dispersion. Interestingly, the *ACH* increase is higher for narrow canyons, i.e. when the configuration is more critical. From the practical point of view, this has two main consequences: firstly, the roof shape have to be considered when assessing the fluid dynamic performances of a UC; secondly, the choice of the roof shape can be a useful tool in the hands of urban planners and building designers to improve the quality of life in urban areas.

Acknowledgements

This work has been financially supported by the University of Cagliari

References

Ahmad, K., Khare, M., Chaudhry, K.K., 2005. Wind tunnel simulation studies on dispersion at urban street canyons and intersections—a review. J. Wind Eng. Ind. Aerodyn. 93, 697–717. doi:10.1016/j.jweia.2005.04.002

Brown, M.J., Lawson, R.E., DeCroix, D.S., Lee, R.L., 2000. Mean flow and turbulence measurements around a 2-D array of buildings in a wind tunnel, in: 11th Joint AMS/AWMA Conference on the Applications of Air Pollution Meteorology. Long Beach, CA.

Di Bernardino, A., Monti, P., Leuzzi, G., Querzoli, G., 2015a. Water-Channel Study of Flow and Turbulence Past a Two-Dimensional Array of Obstacles. Bound.-Layer Meteorol. 155, 73–85. doi:10.1007/s10546-014-9987-2

Di Bernardino, A., Monti, P., Leuzzi, G., Querzoli, G., 2015b. On the effect of the aspect ratio on flow and turbulence over a two-dimensional street canyon. Int. J. Environ. Pollut. 58, 27–38. doi:10.1504/IJEP.2015.076581

Dritselis, C.D., 2014. Large eddy simulation of turbulent channel flow with transverse roughness elements on one wall. Int. J. Heat Fluid Flow 50, 225–239. doi:10.1016/j.ijheatfluidflow.2014.08.008

Fernando, H.J.S., Lee, S.M., Anderson, J., Princevac, M., Pardyjak, E., Grossman-Clarke, S., 2001. Urban Fluid Mechanics: Air Circulation and Contaminant Dispersion in Cities. Environ. Fluid Mech. 1, 107–164. doi:10.1023/A:1011504001479

Franke, J., Hellsten, A., Schlunzen, K.H., Carissimo, B., 2011. The COST 732 Best Practice Guideline for CFD simulation of flows in the urban environment: a summary. Int. J. Environ. Pollut. 44, 419. doi:10.1504/IJEP.2011.038443

Franke, J., Sturm, M., Kalmbach, C., 2012. Validation of OpenFOAM 1.6.x with the German VDI guideline for obstacle resolving micro-scale models. J. Wind Eng. Ind. Aerodyn., 13th International Conference on Wind Engineering 104–106, 350–359. doi:10.1016/j.jweia.2012.02.021

Furuya, Y., Miyata, M., Fujita, H., 1976. Turbulent Boundary Layer and Flow Resistance on Plates Roughened by Wires. J. Fluids Eng. 98, 635–643. doi:10.1115/1.3448434

Hertwig, D., Efthimiou, G.C., Bartzis, J.G., Leitl, B., 2012. CFD-RANS model validation of turbulent flow in a semi-idealized urban canopy. J. Wind Eng. Ind. Aerodyn. 111, 61–72. doi:10.1016/j.jweia.2012.09.003

Ho, Y.-K., Liu, C.-H., Wong, M.S., 2015. Preliminary study of the parameterisation of street-level ventilation in idealised two-dimensional simulations. Build. Environ. 89, 345–355. doi:10.1016/j.buildenv.2015.02.042

Huang, Y., Hu, X., Zeng, N., 2009. Impact of wedge-shaped roofs on airflow and pollutant dispersion inside urban street canyons. Build. Environ. 44, 2335–2347. doi:10.1016/j.buildenv.2009.03.024

Hunter, L.J., Johnson, G.T., Watson, I.D., 1992. An investigation of three-dimensional characteristics of flow regimes within the urban canyon. Atmospheric Environ. Part B Urban Atmosphere 26, 425–432. doi:10.1016/0957-1272(92)90049-X

Hunter, L.J., Watson, I.D., Johnson, G.T., 1990. Modelling air flow regimes in urban canyons. Energy Build. 15, 315–324. doi:10.1016/0378-7788(90)90004-3

Hussain, M., Lee, B.E., 1980. An investigation of wind forces on three dimensional roughness elements in a simulated atmospheric boundary layer flow: part 3: the effect of central model height variations relative to the surrounding roughness arrays. Report BS 57, Department of Building Science University of Sheffield

Jiménez, J., 2004. Turbulent Flows Over Rough Walls. Annu. Rev. Fluid Mech. 36, 173–196. doi:10.1146/annurev.fluid.36.050802.122103

Kastner-Klein, P., Plate, E.J., 1999. Wind-tunnel study of concentration fields in street canyons. Atmos. Environ. 33, 3973–3979. doi:10.1016/S1352-2310(99)00139-9

Launder, B.E., Spalding, D.B., 1974. The numerical computation of turbulent flows. Comput. Methods Appl. Mech. Eng. 3, 269–289. doi:10.1016/0045-7825(74)90029-2

Leonardi, S., Orlandi, P., Antonia, R.A., 2007. Properties of d- and k-type roughness in a turbulent channel flow. Phys. Fluids 19, 125101. doi:10.1063/1.2821908

Leonardi, S., Orlandi, P., Djenidi, L., Antonia, R.A., 2004. Structure of turbulent channel flow with square bars on one wall. Int. J. Heat Fluid Flow, Turbulence and Shear Flow Phenomena (TSFP-3) 25, 384–392. doi:10.1016/j.ijheatfluidflow.2004.02.022

Liu, C.-H., Leung, D.Y.C., Barth, M.C., 2005. On the prediction of air and pollutant exchange rates in street canyons of different aspect ratios using large-eddy simulation. Atmos. Environ. 39, 1567–1574. doi:10.1016/j.atmosenv.2004.08.036

Liu, C.-H., Ng, C.-T., Wong, C.C.C., 2015. A theory of ventilation estimate over hypothetical urban areas. J. Hazard. Mater. 296, 9–16. doi:10.1016/j.jhazmat.2015.04.018

Louka, P., Belcher, S. E., Harrison R.G., 2000. Coupling between air flow in streets and the well-developed boundary layer aloft, Atm. Env., 34, 2613-2621.

Neophytou, M.K.-A., Markides, C.N., Fokaides, P.A., 2014. An experimental study of the flow through and over two dimensional rectangular roughness elements: Deductions for urban boundary layer parameterizations and exchange processes. Phys. Fluids 1994-Present 26, 86603. doi:10.1063/1.4892979

Ng, E., 2009. Policies and technical guidelines for urban planning of high-density cities – air ventilation assessment (AVA) of Hong Kong. Build. Environ., The 6th International Conference on Indoor Air Quality, Ventilation &Energy Conservation in Buildings (IAQVEC 2007), Sendai, Japan, 28-31 October, 2007 44, 1478–1488. doi:10.1016/j.buildenv.2008.06.013

Oke, T.R., 1988. Street design and urban canopy layer climate. Energy Build. 11, 103–113. doi:10.1016/0378-7788(88)90026-6

Ozmen, Y., Baydar, E., van Beeck, J.P.A.J., 2016. Wind flow over the low-rise building models with gabled roofs having different pitch angles. Build. Environ. 95, 63–74. doi:10.1016/j.buildenv.2015.09.014

Patankar, S.., Spalding, D.., 1972. A calculation procedure for heat, mass and momentum transfer in three-dimensional parabolic flows. Int. J. Heat Mass Transf. 15, 1787–1806. doi:10.1016/0017-9310(72)90054-3

Perry, A.E., Schofield, W.H., Joubert, P.N., 1969. Rough wall turbulent boundary layers. J. Fluid Mech. 37, 383–413. doi:10.1017/S0022112069000619

Rafailidis, S., 1997. Influence of Building Areal Density and Roof Shape on the Wind Characteristics Above a Town. Bound.-Layer Meteorol. 85, 255–271. doi:10.1023/A:1000426316328

Sini, J.-F., Anquetin, S., Mestayer, P.G., 1996. Pollutant dispersion and thermal effects in urban street canyons. Atmos. Environ. 30, 2659–2677. doi:10.1016/1352-2310(95)00321-5

Snyder, W.H., 1981. Guideline for fluid modeling of atmospheric diffusion. Environmental Sciences Research Laboratory, Office of Research and Development, US Environmental Protection Agency.

Takano, Y., Moonen, P., 2013. On the influence of roof shape on flow and dispersion in an urban street canyon. J. Wind Eng. Ind. Aerodyn. 123, Part A, 107–120. doi:10.1016/j.jweia.2013.10.006

Tominaga, Y., Mochida, A., Yoshie, R., Kataoka, H., Nozu, T., Yoshikawa, M., Shirasawa, T., 2008. AIJ guidelines for practical applications of CFD to pedestrian wind environment around buildings. J. Wind Eng. Ind. Aerodyn., 4th International Symposium on Computational Wind Engineering (CWE2006) 96, 1749–1761. doi:10.1016/j.jweia.2008.02.058

Weller, H.G., Tabor, G., Jasak, H., Fureby, C., 1998. A tensorial approach to computational continuum mechanics using object-oriented techniques. Comput. Phys. 12, 620–631. doi:10.1063/1.168744

Xie, X., Huang, Z., Wang, J., 2005. Impact of building configuration on air quality in street canyon. Atmos. Environ. 39, 4519–4530. doi:10.1016/j.atmosenv.2005.03.043

Yakhot, V, S. A. Orszag, 1986. Renormalization group analysis of turbulence. I. Basic theory. J. Sci. Comput. 1, 3-51. doi:10.1007/BF01061452.

Yassin, M.F., 2011. Impact of height and shape of building roof on air quality in urban street canyons. Atmos. Environ. 45, 5220–5229. doi:10.1016/j.atmosenv.2011.05.060

Yazid, A.W.M., Sidik, N.A.C., Salim, S.M., Saqr, K.M., 2014. A review on the flow structure and pollutant dispersion in urban street canyons for urban planning strategies. Simulation 90, 892–916. doi:10.1177/0037549714528046

Zajic, D., Fernando, H.J.S., Calhoun, R., Princevac, M., Brown, M.J., Pardyjak, E.R., 2010. Flow and Turbulence in an Urban Canyon. J. Appl. Meteorol. Climatol. 50, 203–223. doi:10.1175/2010JAMC2525.1

On the effect of gable roof on natural ventilation in two-dimensional urban canyons

Maria Grazia Badas[a], Simone Ferrari[a], Michela Garau[a], Giorgio Querzoli[a]
[a] DICAAR, Università degli studi di Cagliari, , Via Marengo 2, 09128, Cagliari, Italy

Highlights

- Roof pitch improves natural ventilation inside the canyon;
- The effect of the roof slope is more significant in narrow canyons;
- Relation between friction coefficient and turbulent air exchange is independent on pitch;